

# Comparison of Jet Quenching Formalisms for a Quark-Gluon Plasma “Brick” (Outline Version II)

TEC-HQM Collaboration

*The Earth, Solar System, Milky Way, Virgo Supercluster, Universe*

(Dated: July 12, 2009)

This is the second draft of the outline of a report describing the comparison of various pQCD based formalisms treating the energy loss of hard partons in a thermal quark-gluon plasma for a simplified geometry. Specifically, we compare the predictions of the WHDG and ASW, and Higher Twist (HT) formalisms in the opacity expansion, and of the BDMPS-Z and AMY formalisms in the multiple soft scattering approximation.

## I. JET QUENCHING FORMALISMS: OVERVIEW

The first section contains an introductory review of the theory of jet quenching in perturbative QCD. It discusses collisional and radiative energy loss, and gives a brief overview of the major formalisms for radiative energy loss: BDMPS-Z and AMY in the multiple-soft scattering limit applicable to a “thick” medium, WHDG/GLV, ASW, and Higher Twist (HT) in the opacity expansion applicable to a “thin” medium.

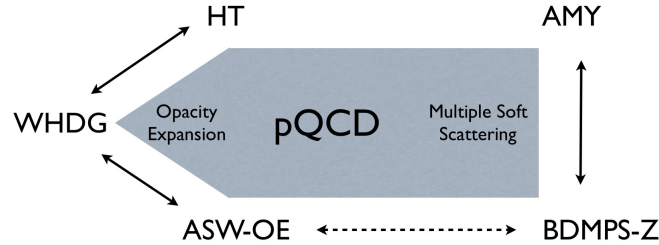


FIG. 1: The landscape of pQCD based jet quenching formalisms. Arrows indicate pairs of formalisms for which detailed analytical and numerical comparisons are presented.

## II. THE QUARK-GLUON PLASMA “BRICK” CHALLENGE

This section describes the “QGP Brick” challenge as formulated in the TEC-HQM Wiki. Definition of the “original brick” and the “Wiedemann brick”, as well as the definition and motivation of the “observable”  $R_8$ .

## III. DETAILED COMPARISONS OF MODELS

### A. WHDG and ASW–OE

[Coordinated by William Horowitz and Brian Cole.]

#### 1. Introduction

In this section we will (1) make detailed comparisons of the radiative part of the WHDG calculation [? ], namely DGLV [? ], with ASW-SH [? ], (2) discuss the importance of the definition of  $x$  and the kinematic cutoffs used to enforce the assumptions used in deriving the energy loss formulae, and (3) give quantitative brick results comparing the radiative and elastic components of WHDG.

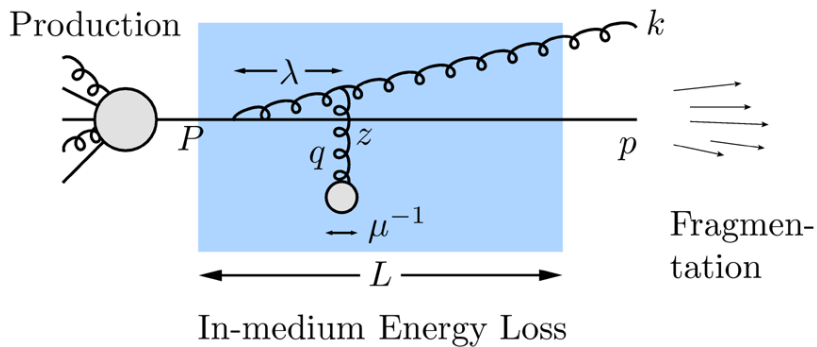


FIG. 2: (Color online) Cartoon of the production, in-medium energy loss, and fragmentation processes that may occur perturbatively for a high- $p_T$  parton produced in a heavy ion collision. The labels are  $P$  for the initial parent parton momentum,  $p$  for its final momentum,  $k$  for the medium-induced bremsstrahlung gluon momentum, and  $q$  for the momentum transfer between an in-medium scattering center and the high- $p_T$  parent parton.

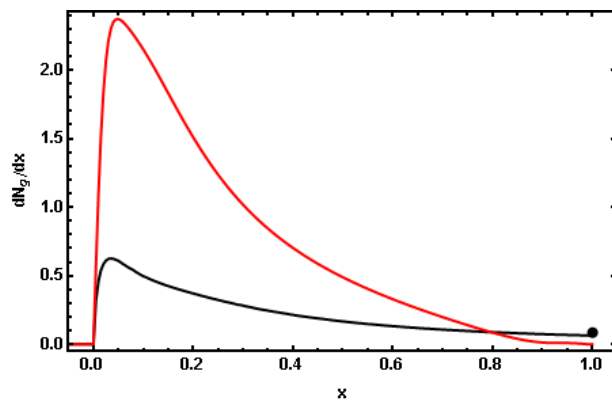


FIG. 3: Plot of the single inclusive gluon radiation distribution,  $dN_g/dx$ , from the WHDG implementation of the first order in opacity DGLV formula, Eq. (1), in red, and the ASW-SH implementation of Eq. (2), in black, for a 10 GeV up quark traversing a nominal, 2 fm long static brick of QGP held at a constant  $T = 485$  MeV. The point at  $x = 1$  indicates the integrated weight of  $dN_g/dx$  in the ASW-SH implementation for  $x > 1$ .

## 2. Making GLV=ASW-SH and Model Implementation

One of the major driving forces in the creation of the TECHQM collaboration was the realization that not only do the physics assumptions made in a derivation have an impact on the predictions of experimental observables such as  $R_{AA}$  but also all the modeling assumptions. An excellent case in point comes when one attempts a naive comparison between the single inclusive gluon distribution implemented in a massless quark and gluon version of the radiative piece of WHDG and the one found from the ASW-SH code [?] for the opacity expansion (see Fig. 2 for a cartoon of the perturbative process and definitions of symbols we will use throughout the section). Both purport to compute the single inclusive distribution of gluon radiation,  $dN_g/dx$ , to first order in opacity [? ? ?] for a medium of Debye-screened colored static scattering centers [?]. See Fig. 3, which shows  $dN_g^{\text{WHDG-Rad}}/dx$  and  $dN_g^{\text{ASW-SH}}/dx$  for a nominal 10 GeV quark jet in a static,  $T = 485$  MeV plasma of length 2 fm[1]. The DGLV formula for the first order in opacity energy loss is [?]:

$$x \frac{dN_g^{\text{DGLV}}}{dx} = \frac{2C_R \alpha_s L}{\pi^3 \lambda} \int d^2 \mathbf{q} d^2 \mathbf{k} \frac{\mu^2}{(\mathbf{q}^2 + \mu^2)^2} \frac{\mathbf{k} \cdot \mathbf{q} (\mathbf{k} - \mathbf{q})^2 - \beta^2 \mathbf{q} \cdot (\mathbf{k} - \mathbf{q})}{[(\mathbf{k} - \mathbf{q})^2 + \beta^2]^2 (\mathbf{k}^2 + \beta^2)} \int dz \left[ 1 - \cos \left( \frac{(\mathbf{k} - \mathbf{q})^2 + \beta^2}{2xE} z \right) \right] \rho(z), \quad (1)$$

where  $\beta^2 = m_g^2 + x^2 M_q^2$  (with  $m_g$  the effective thermal mass of the radiated gluon and  $M_q$  the mass of the radiating parent parton) and  $\rho(z)$  is the probability distribution for the distance to the first scattering center[2]. Alternatively

the result for ASW-SH [? ], which does not include the effect of a thermal gluon mass, is:

$$\omega \frac{dI^{ASW-SH}}{d\omega} = \frac{2C_R\alpha_s}{\pi^3} \frac{L}{\lambda} \int d^2\mathbf{q} d^2\mathbf{k} \frac{\mu^2}{(\mathbf{q}^2 + \mu^2)^2} \frac{\mathbf{k} \cdot \mathbf{q}(\mathbf{k} - \mathbf{q})^2 - x^2 M_q^2 \mathbf{q} \cdot (\mathbf{k} - \mathbf{q})}{[(\mathbf{k} - \mathbf{q})^2 + x^2 M_q^2]^2 (\mathbf{k}^2 + x^2 M_q^2)} \int dz \left[ 1 - \cos \left( \frac{(\mathbf{k} - \mathbf{q})^2 + x^2 M_q^2}{2\omega} \right) \right] \rho(z). \quad (2)$$

If we take  $\omega = xE$  (this will be discussed further below) in Eq. (2) and  $m_g = 0$  in  $\beta$  in Eq. (1), then we see that Eqs. (1) and (2) are, in fact, identical! So what happened between the formulae, Eqs. (1) and (2), and the curves in Fig. 3? Implementation. It turns out that there are a number of decisions that one must make in going from the highly differential equations to their integrated result,  $dN_g/dx$ . These are summarized in Table I.

	WHDG	ASW-SH
$k_{\max}$	$2x(1-x)E$	$xE$
$x$	$x_+$	$x_E$
$q_{\max}$	$\sqrt{3\mu E}$	$\infty$
$\rho(z)$	$2e^{-2z/L}\theta(z)/L$	$\theta(L-z)\theta(z)/L$
$L/\lambda$	$L\rho\sigma = L\rho \times 9\pi\alpha_s^2/(2\mu^2)$	1
$\alpha_s$	0.3	1/3
$m_g; M_q$	$\mu/\sqrt{2}; \mu/2$	0; 0

TABLE I: Table of differences between the implementation of Eqs. (1) and (2) in WHDG and in ASW-SH.

If one alters the radiative energy loss part of WHDG to have all the assumptions used in the ASW-SH code, then one finds agreement within numerical precision; see the Top Left plot in Fig. 4. In this case one

- Sets the thermal gluon mass to 0.
- Sets the thermal quark mass to 0.
- Uses  $k_{\max} = xE$ , where  $k_{\max}$  is the maximum allowed value of  $k_T = |\mathbf{k}|$ .
- Uses the ASW scattering center distribution.
- Fixes  $L/\lambda = 1$ .
- Uses  $q_{\max} = \infty$ .
- Uses  $\alpha_s = 1/3$ .

One can see from Figs. 4 and 5 the quantitative progression from exact agreement when the same assumptions are made to the result observed in Fig. 3. The progression systematically removes the changes given in the above list in reverse order. There are numerous lessons to be learned from Figs. 4 and 5. That the changes in  $\alpha_s$ ,  $M_q$ , and  $q_{\max}$  lead to small differences in  $dN_g/dx$  is not a surprise:  $\alpha_s$  differs by only 10%;  $M_q$  for WHDG is small; and it has been known for a long time that  $dN_g/dx$  is not sensitive to changes in  $q_{\max}$ . Also not surprising is the huge difference when  $L/\lambda$  is allowed to vary. While at the level of  $dN_g/dx$  one can simply scale the results to account for a varying  $L/\lambda$ , this is not true once the distribution has been folded multiple times into a Poisson convolution; note that the ASW-SH code [? ] only gives the Poisson convolution results. The differences seen in the  $dN_g/dx$  from the two scattering center distributions seems to suggest only a small dependence on their exact form. The apparent huge sensitivity to the inclusion of a radiated gluon mass,  $m_g$ , is a surprise. However, due to nontrivial interference effects, its affect on observables such as  $R_{AA}$  are actually not particularly large [? ].

### 3. Interpretations of $x$ and Importance of Cutoffs

The very large changes seen when going from the two numerically different  $k_{\max}$  values is a surprise given the assumption of collinearity used in the derivation of the energy loss formulae, Eqs. (1) and (2), and warrants further explanation. Collinearity,  $k_T \ll xE$ , is the assumption that radiation is emitted at small angles. To further investigate collinearity, it is necessary to discuss the specific definition of  $x$  further. It turns out that, as noted in the table, the GLV-descended derivations [? ? ? ? ] interpret  $x = x_+ = k^+/P^+$  as the fraction of light-cone plus momentum carried away by the radiated gluon. On the other hand the ASW-SH derivation [? ? ] defined  $x = x_E = k^0/P^0$  as

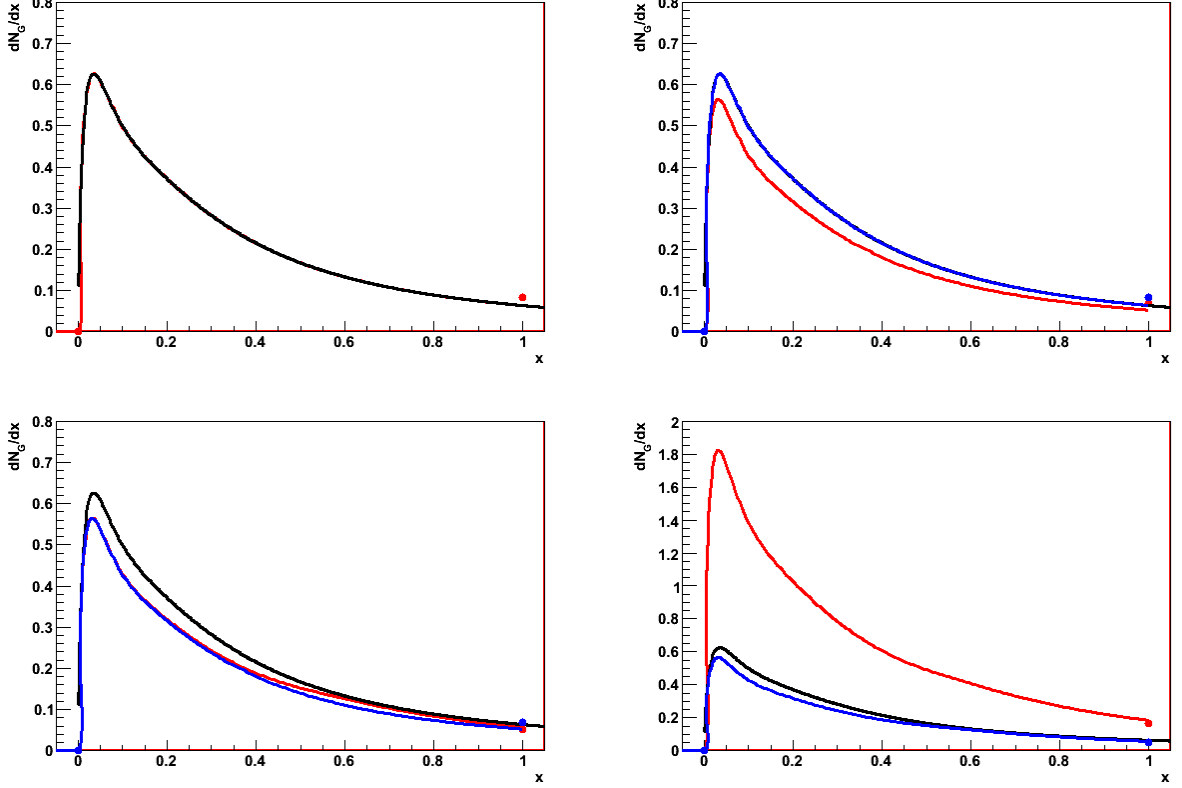


FIG. 4: First half of the progression from ASW-SH to the radiative piece of WHDG. The black curve in all figures represents ASW-SH. The red curve in each figure represents the result when the next progressive change away from WHDG is removed. To aid comparison, the result from the previous plot is shown in blue. Dots at  $x = 1$  represent the integrated weight of  $dN_g/dx$  for  $x > 1$ . Progression proceeds as follows: (Top Left) exact reproduction of ASW-SH (within numerical precision); (Top Right)  $\alpha_s = 1/3$  to  $\alpha_s = 0.3$ ; (Bottom Left)  $q_{\max} = \infty$  to  $q_{\max} = \sqrt{3\mu E}$ ; (Bottom Right)  $L/\lambda = 1$  to  $L/\lambda = L\rho\sigma = 9\pi\alpha_s^2\rho L/(2\mu^2)$ .

the fraction of energy carried away by the radiated gluon. If we denote the usual four-momenta with parentheses and light-cone momenta with brackets then the on mass shell radiated gluon momentum is

$$k = (x_E E, \sqrt{(x_E E)^2 - \mathbf{k}^2}, \mathbf{k}) = [x_+ E^+, \frac{\mathbf{k}^2}{x_+ E^+}, \mathbf{k}], \quad (3)$$

where  $\mathbf{k}$  is the momentum of the gluon transverse to the direction of the parent parton. Similarly, the momentum for an on mass shell massless parent parton is

$$p = ((1 - x_E)E, \sqrt{((1 - x_E)E)^2 - (\mathbf{q} - \mathbf{k})^2}, \mathbf{q} - \mathbf{k}) = [(1 - x_+)E^+, \frac{(\mathbf{q} - \mathbf{k})^2}{(1 - x_+)E^+}, \mathbf{q} - \mathbf{k}], \quad (4)$$

where  $\mathbf{q}$  is the transverse momentum transfer to the parent parton from the in-medium scattering center. (For completeness the original parent parton momentum is  $P = (E, E, \mathbf{0}) = [E^+, 0, \mathbf{0}]$ .) Using Eqs. (3) and (4) one may derive the exact relationships between  $x_+$  and  $x_E$ :

$$x_+ = \frac{1}{2} x_E \left( 1 + \sqrt{1 - \left( \frac{k_T}{x_E E} \right)^2} \right), \quad (5)$$

$$x_E = x_+ \left( 1 + \left( \frac{k_T}{x_+ E^+} \right)^2 \right), \quad (6)$$

Note that to lowest order in collinearity, where the (assumed small) expansion parameter is  $k_T/x_E$ , the two definitions of  $x$  given above are identical.

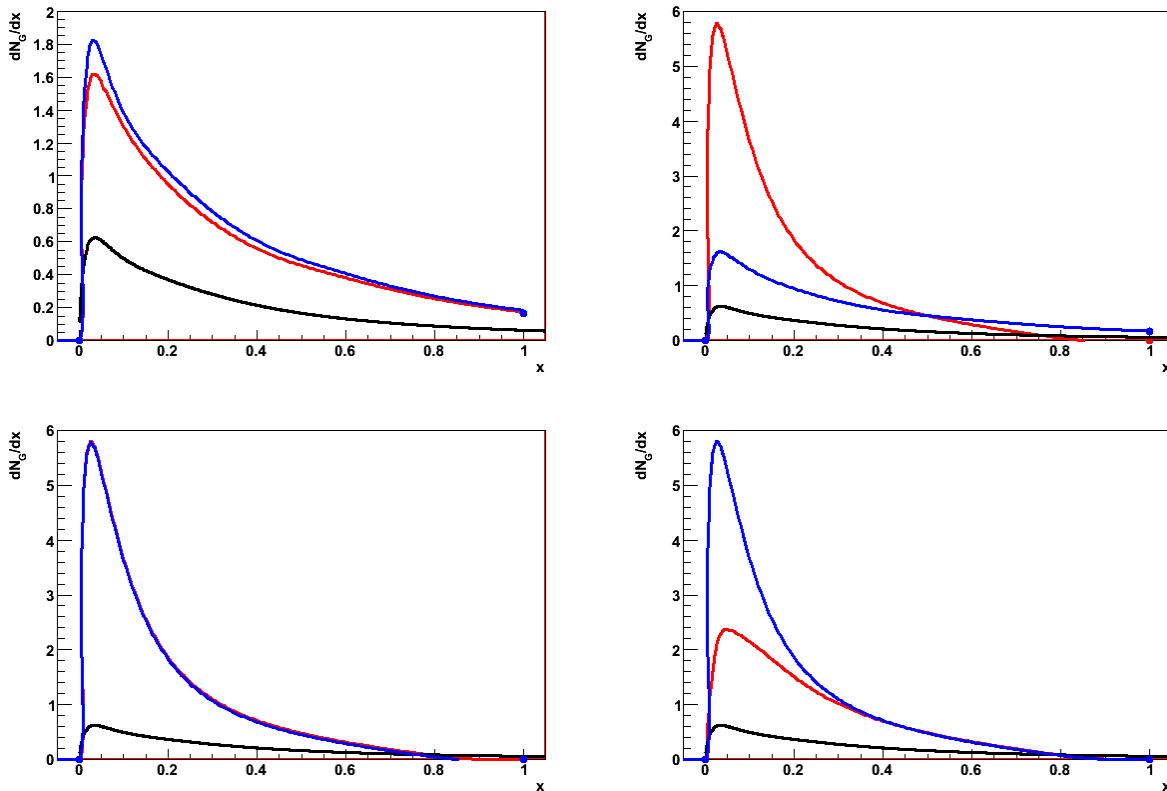


FIG. 5: Second half of the progression from ASW-SH to the radiative piece of WHDG. The black curve in all figures represents ASW-SH. The red curve in each figure represents the result when the next progressive change away from WHDG is removed. To aid comparison, the result from the previous plot is shown in blue. Dots at  $x = 1$  represent the integrated weight of  $dN_g/dx$  for  $x > 1$ . Progression proceeds as follows: (Top Left)  $\rho(z) = \theta(L-z)\theta(z)/L$  to  $\rho(z) = 2e^{-2z/L}\theta(z)/L$ ; (Top Right)  $k_{\max} = xE$  to  $k_{\max} = 2x(1-x)E$ ; (Bottom Left)  $M_q = 0$  to  $M_q = \mu/2$ ; (Bottom Right)  $m_g = 0$  to  $m_g = \mu/\sqrt{2}$ .

A number of assumptions are made in the process of deriving Eqs. (1) and (2) in order to simplify the analytics. Specifically one makes assumptions of: (1) eikonicity (i.e. high energy,  $E$ ); (2) soft radiation,  $x \ll 1$ ; (3) collinearity,  $k_T \ll xE$ ; (4) parent parton pathlength much longer than the mean free path of the gluon in medium,  $L \gg \lambda$ . Note that all these assumptions are also made in the BDMPS and AMY formalisms[3]. HT makes all these assumptions except for (2). It is worth emphasizing that all current pQCD-based energy loss calculations make the assumption of collinearity.

A simple examination of Eqs. (1) and (2) shows that these equations do not “know about” the assumptions made in their derivation; they do not naturally die out when the approximations used in their derivation break down. As one example, they have support for all  $k_T$ . Collinearity has traditionally been enforced through the requirement of forward emission, by cutting off the  $k_T$  integration for  $dN_g/dx$  in the UV. In light cone coordinates forward emission implies that  $k^+ > k^-$ . This condition yields

$$k_T < k_{\max} = x_+ P^+ = x_+ E^+. \quad (7)$$

In Minkowski coordinates forward emission implies that  $k^z > 0$ . This condition leads to

$$k_T < k_{\max} = x_E E. \quad (8)$$

However, requiring forward emission only restricts emission to angles less than  $90^\circ$ , which is still a rather wide angle. One may go further, in anticipation of exploring the sensitivity of results to variations in the  $k_T$  cutoff, and define an angle,  $\theta_{\max}$ , with radiation emission not permitted for angles larger than  $\theta_{\max}$ . Using this as a cutoff criteria yields

$$k_{\max} = \begin{cases} x_+ E^+ \tan(\theta_{\max}/2), & x = x_+, \\ x_E E \sin(\theta_{\max}), & x = x_E. \end{cases} \quad (9)$$

Eqs. (1) and (2) also have support for all values of  $x$ . Nonzero weight for  $dN_g/dx$  for  $x > 1$  of course violates energy-momentum conservation. Requiring the continued forward propagation of the parent parton leads to an additional  $k_T$  cutoff that minimally enforces energy-momentum conservation while simultaneously enforcing consistency with the assumption of eikonicity. In light cone coordinates forward propagation implies  $p^+ > p^-$ ; in Minkowski coordinates one requires  $k^z > 0$ . For the light cone coordinate case forward emission leads to

$$(1 - x_+)E^+ > |\mathbf{q} - \mathbf{k}| \approx k_T, \quad (10)$$

where  $q \sim 3T < q_{\max} = \sqrt{6ET}$  is small compared to most values of  $k = |\mathbf{k}|$ ; for the Minkowski coordinate case forward emission leads to

$$(1 - x_E)E > |\mathbf{q} - \mathbf{k}| \approx k_T. \quad (11)$$

For each  $x$  interpretation there are two cutoffs (e.g. Eqs. (7) and (10) for the  $x = x_+$  interpretation or Eqs. (8) and (11) for the  $x = x_E$  interpretation); one should then take this into account when evaluating the  $k_T$  integral of  $dN_g/dxdk_T$ . One possibility would be to take the minimum of the two; for instance, using light cone coordinates and taking  $\theta_{\max} = \pi/2$  this would mean  $k_{\max} = \min(x_+, 1 - x_+)E^+$ . DGLV (and WHDG) use a smoother function, namely  $k_{\max} = x_+(1 - x_+)E^+$ . Note that the ASW-SH implementation [?] does not include a large  $x$  cutoff. One could of course do the same  $\theta_{\max}$  analysis for the large  $x$  cutoff. However one can see from Fig. 6 that the  $dN_g/dx$  distribution is actually rather insensitive to this cutoff; in this sense the  $dN_g/dxdk_Tdq_T$  integrand respects the small  $x$  approximation rather well.

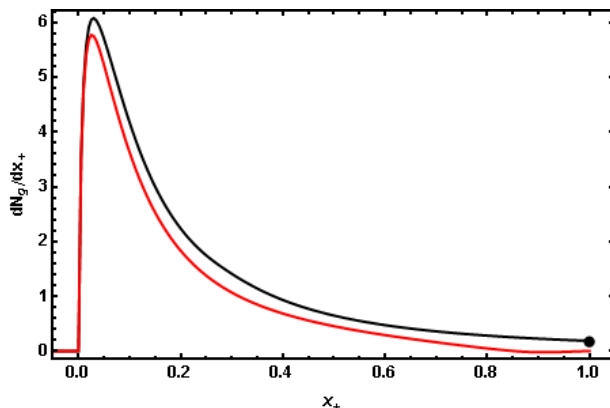


FIG. 6: Plots comparing the result for Eq. (1) with  $k_{\max} = x_+E^+$  (black) and  $k_{\max} = x_+(1 - x_+)E^+$  (red) cutoffs for a 10 GeV up quark traversing a 2 fm static QGP of  $T = 485$  MeV. Enforcing the small  $x$  approximation, and simultaneously enforcing energy and momentum conservation at the level of  $dN_g/dx$ , does not make a large difference to the emission spectrum. The black dot at  $x_+ = 1$  represents the integrated weight of  $dN_g/dx_+$  for  $x_+ > 1$  when  $k_{\max} = x_+E^+$ .

Fig. 7 plots  $dN_g/dxdk_T$  along with an illustration of three possible cutoffs for  $k_T$ : (1)  $x = x_+$  with  $\theta_{\max} = \pi/2$ , (2)  $x = x_E$  with  $\theta_{\max} = \pi/2$ , and (3)  $x = x_E$  with  $\theta_{\max} = \pi/4$ . Recall that to lowest order in collinearity, the first two cutoffs are identical; the third is a natural  $\mathcal{O}(1)$  variation in the cutoff that one can use to estimate the systematic theoretical uncertainties coming from the collinear approximation. Clearly the assumption of collinearity is badly, even maximally violated; for values of  $x \sim \mu/E$ ,  $dN_g/dxdk_T$  reaches its maximum value at  $k_T \sim xE$ . For these values of  $x$  the emission spectrum is highly sensitive to the particular value of  $k_{\max}$  chosen;  $dN_g/dx \sim k_{\max}^2$ .

Since the collinear approximation is so badly broken, it is not a good approximation to take  $x_+ \approx x_E$ . A meaningful ‘‘apples-to-apples’’ comparison of results, then, can come only when the emission spectra of Eqs. (1) and (2) are plotted using the same variables. Since one is interested in a differential quantity, a Jacobian is required. We choose to transform  $x_+$  to  $x_E$  because, ultimately, one is interested in energy, as opposed to light-cone plus momentum, loss. In this case the transformed spectrum is given by

$$\frac{dN_g^J}{dx_E}(x_E) \equiv \int^{x_E E \sin(\theta_{\max})} dk_T \frac{dx_+}{dx_E} \frac{dN_g}{dx_+ dk_T}(x_+(x_E)), \quad (12)$$

$$\frac{dx_+}{dx_E} = \frac{1}{2} \left[ 1 + \left( 1 - \left( \frac{k_T}{x_E E} \right)^2 \right)^{-1} \right]. \quad (13)$$

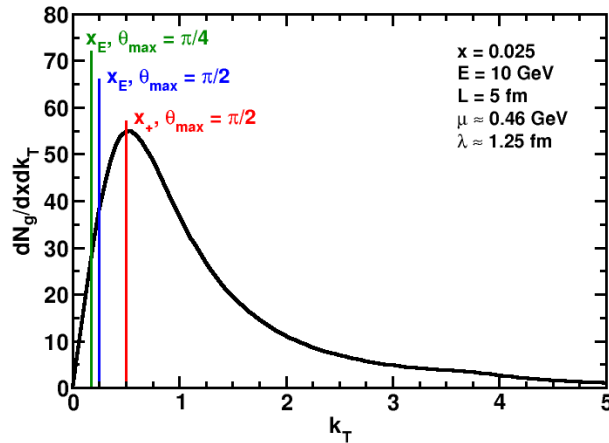


FIG. 7: Plot of  $dN_g/dxdk_T$  from Eq. (1) for a light quark with all masses set to 0,  $E = 10$  GeV,  $L = 5$  fm, and representative values of  $\mu \simeq 0.46$  GeV and  $\lambda \simeq 1.25$  fm for a medium density of  $dN_g/dy = 1000$  similar to RHIC conditions [? ]. Vertical lines depict the three values of  $k_T$  discussed in the text as possible cutoffs to enforce collinearity in Eq. (1). Note that with  $x = 0.025 \sim \mu/E$ ,  $dN_g/dxdk_T$  is maximized near  $k_T \sim k_{\max}$ , completely in contradiction to the collinear approximation.

Note the change in the upper limit of integration in Eq. (12) as dictated by the basic rules of calculus. An “apples-to-apples” comparison of  $dN_g/dx_E$  is shown in Fig. 8. Note the very large difference in results for the two collinearly equivalent definitions of  $x$  and that for the result with a reduced  $\theta_{\max}$ . Of course this enormous difference leads to extremely large systematic theoretical errors ( $\sim 200\%$ ) in the extraction of medium parameters [? ].

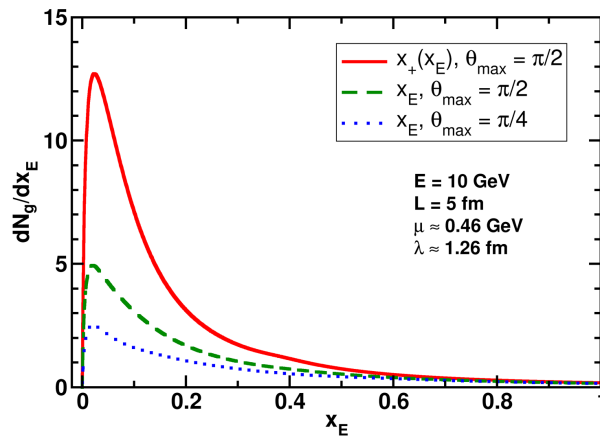


FIG. 8: “Apples-to-apples” comparison of Eqs. (1) and (2) in the massless limit and for which the  $x_+$  dependence of Eq. (1) has been transformed into  $x_E$ ; see Eq. (12). Also shown is the result when using the  $x_E$  interpretation and reducing  $\theta_{\max}$  to  $\pi/4$ , a reasonable  $\mathcal{O}(1)$  variation in the  $k_T$  cutoff.

It is worth noting that the usual prescription for the Poisson convolution leads to a distribution that does not conserve energy as the momentum of the parent parton is not dynamically updated. Additionally the convolution, because  $\langle N_g \rangle$  is almost always greater than 1, almost always pushes the mean energy loss  $\langle \epsilon \rangle$  to values larger than the mean value of  $x$  from  $dN_g/dx$ ; therefore the Poisson convolution actually enhances the sensitivity of energy loss calculations to the larger regions of  $x$  for which the derivations are not well controlled theoretically.

#### 4. WHDG Brick Results

In this section we compile the WHDG brick results.

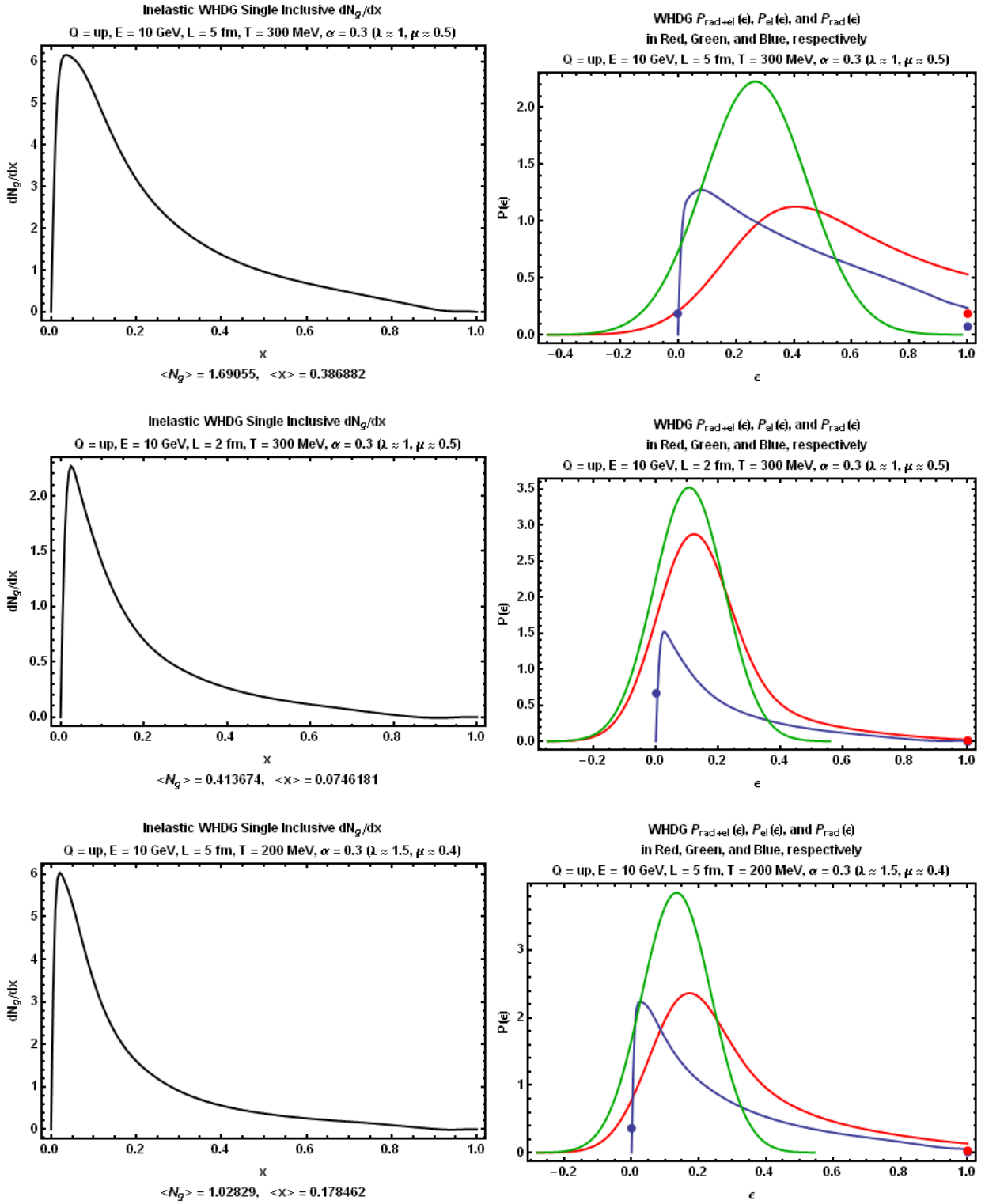


FIG. 9: Results from WHDG for the Original Brick problem.

### B. HT and WHDG

In this section, we describe the radiative part of the higher twist (HT) calculation as applied to the “brick problem”. In short, the higher twist calculation consists of including a class of medium corrections to the process of jet evolution

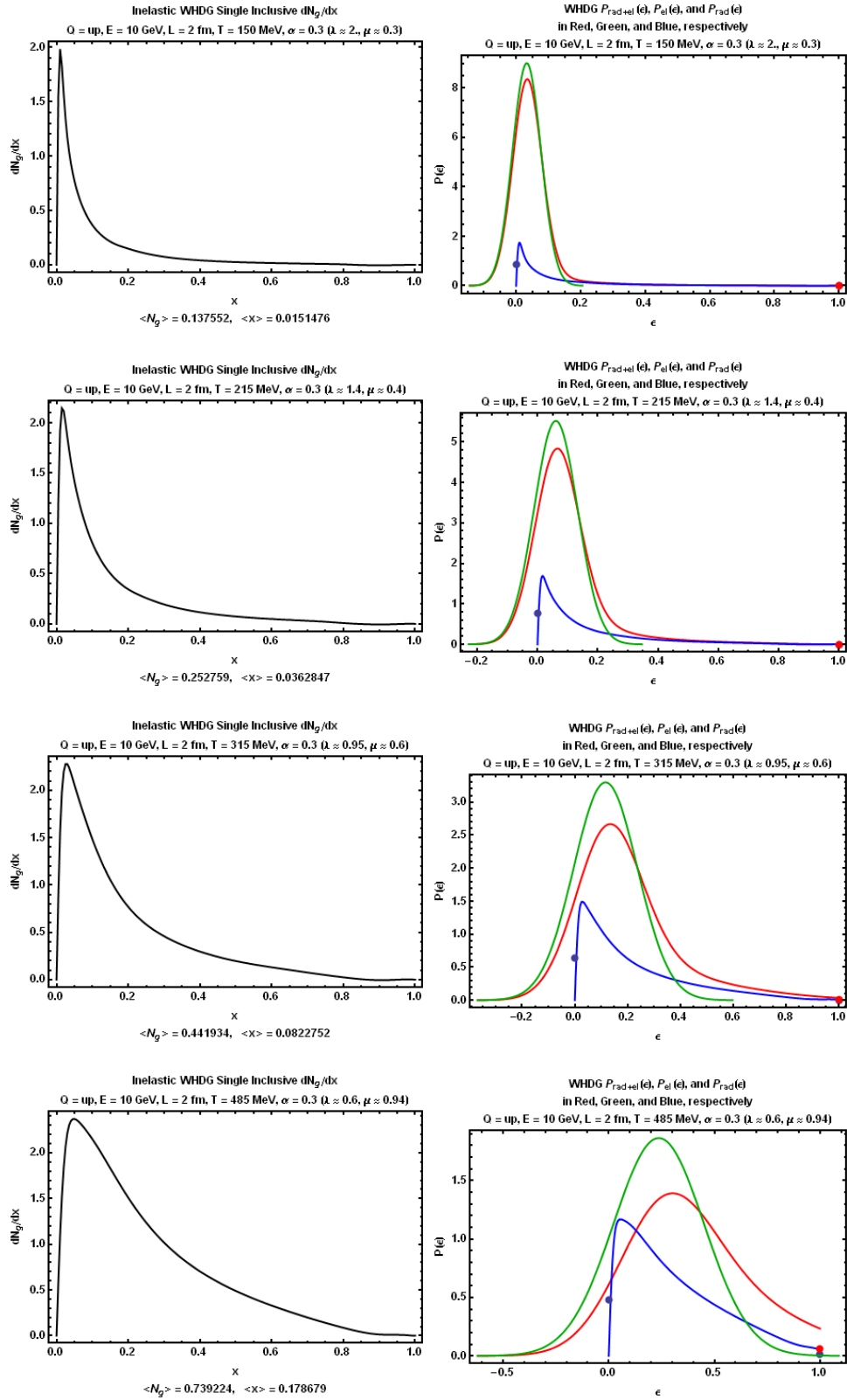


FIG. 10: Results from WHDG for the Wiedemann-Brick problem.

in vacuum, brought about by the multiple scattering of the hard partons in a medium. It is most straightforwardly derived for the case of Single inclusive Deep-Inelastic Scattering (SIDIS) in a large nucleus, with the nucleus playing

the role of the medium. While most scattering corrections are always suppressed by powers of the hard scale  $Q^2$ , a subset of these are enhanced by the length of the medium and these are included in the calculation. Thus, the expansion parameter in the HT is  $\alpha_S \hat{q} L / Q^2$  where  $\hat{q}$  is the transverse momentum squared imparted to a single parton per unit length and  $L$  is the length traversed by the parton.

Consider the case of DIS on a nucleon (in the Breit frame). The nucleus has a large momentum in the positive light cone direction  $A[p^+, 0, 0, 0]$  with  $p^+$  the mean momentum of a nucleon. The incoming virtual photon has a momentum which may always be expressed as  $[-Q^2/2q^-, q^-, 0, 0]$ ; in the Breit frame  $q^- = Q/\sqrt{2}$ . The inclusive cross section to produce a hard hadron, which carries a momentum fraction  $z$  of the initial produced hard quark may be expressed in a factorized form as,

$$\frac{d\sigma}{dz} = \int dx G(x, Q^2) \frac{d\hat{\sigma}}{dQ^2} D(z, Q^2), \quad (14)$$

where,  $G(x)$  is the parton distribution function (PDF) to obtain a hard quark in the nucleon with momentum fraction  $x$ . In the Breit frame the momentum of the incoming quark is  $xp^+ = Q/\sqrt{2}$ . Thus the produced quark has an outgoing momentum  $q^- = Q/\sqrt{2}$ . The produced quark is virtual with a virtuality smaller than the hard scale usually denoted as  $\lambda Q$  where  $\lambda \ll 1$ . The other two factors are the hard partonic cross section  $\frac{d\hat{\sigma}}{dQ^2}$  and the final fragmentation function  $D(z, Q^2)$ . The scale in the fragmentation function is the factorization scale and also represents the maximum possible virtuality of the produced hard jet. The fragmentation function at the scale  $Q$  may be obtained from a measured fragmentation function at a lower scale using the DGLAP evolution equations,

$$\frac{\partial D_q^h(z, Q^2)}{\partial \log(Q^2)} = \frac{\alpha_S(Q^2)}{2\pi} \int_z^1 \frac{dy}{y} P_{qi}(y) D_i^h\left(\frac{z}{y}, Q^2\right). \quad (15)$$

There is an implied sum over  $i$  which includes all possible parton that may split off from the hard leading quark denoted as  $q$ .

In the case of DIS on a large nucleus, the above factorized form may be assumed to hold with the only change being the replacement of the vacuum evolved fragmentation function with a medium modified fragmentation function (as well as a replacement of the nucleon PDF with a nuclear PDF). The medium modified fragmentation function contains the usual vacuum evolution piece Eq. (15) and a medium piece which includes both terms which are interferences between medium induced radiation and vacuum radiation as well as terms where both the amplitude and the complex conjugate represent medium induced radiation. Once so factorized, the medium modified fragmentation function can be used to compute the single hadron inclusive cross section in any process by simply replacing the initial state parton distribution and hard cross section by those appropriate for the process in question.

For calculations in the brick, we simply ignore all the initial state functions and hard cross sections. We assume that the quark is produced at one edge of the brick designated as the origin and travels in the negative light cone direction with a negative light cone momentum  $q^-$ . We assign the quark an initial virtuality  $Q^2$ . Since this is not the Breit frame in DIS there is no implied relation between  $q^-$  and  $Q^2$ . The equation for the medium modified fragmentation function with an initial LC momentum  $q^-$ , virtuality  $Q^2$ , which starts at the location  $\zeta_i^-$  and exits at  $\zeta_f^-$  is given as,

$$\frac{\partial D_q^h(z, Q^2, q^-)|_{\zeta_i^-}^{\zeta_f^-}}{\partial \log(Q^2)} = \frac{\alpha_S}{2\pi} \int_z^1 \frac{dy}{y} \int_{\zeta_i}^{\zeta_f} d\zeta P(y) K_{q^-, Q^2}(y, \zeta) D_q^h\left(\frac{z}{y}, Q^2, q^- y\right) \Big|_{\zeta}^{\zeta_f}. \quad (16)$$

In the equation above, we have dropped the  $(-)$ -superscripts on the positions. Note that the medium modified fragmentation function is now, not only a function of  $Q^2$  and  $z$  but also a function of  $q^-$  and  $\zeta$ . The calculation of the evolution equation now requires the evolution of a three dimensional matrix (in  $z, q^-, \zeta$ ). The medium kernel  $K_{q^-, Q^2}(y, \zeta)$  for a quark jet is given as

$$K_{q^-, Q^2}(y, \zeta) = \left\{ \hat{q}(\zeta) - (1-y)\frac{\hat{q}}{2} + (1-y)^2 \hat{q}_Q \right\} \left[ 2 - 2 \cos \left\{ \frac{Q^2(\zeta - \zeta_i)}{2q^- y(1-y)} \right\} \right]. \quad (17)$$

In the soft gluon approximation  $y \rightarrow 1$ , one only keeps the first factor of  $\hat{q}$  in the equation above. In this limit, the case of a gluon medium modified fragmentation function is obtained by replacing the vacuum splitting function with the two vacuum splitting functions for a gluon: for a gluon to two gluons and a gluon to quark anti-quark. This is so far an unverified assumption. Even at this level of approximation, the equations above are far to numerically intensive to solve. One usually replaces the position dependence with the initial position  $\zeta \rightarrow \zeta_i$ . The evolution equations now represent the evolution of a two dimensional matrix and these represent the calculations which will be

presented in this paper. A further approximation is to also drop the energy dependence and is sometimes presented in the literature.

The first set of plots represent the default HT calculation which is the medium fragmentation function for a  $\pi^0$ . The jet is assumed to have energies 20 GeV and 100 GeV and goes through a medium of length 2 fm and 5 fm. The initial virtuality of the jet for the case of 20 GeV is set to be 100 GeV<sup>2</sup> and for the case of 100 GeV to be 2500 GeV<sup>2</sup>.

### C. AMY and BDMPS-Z

[Coordinated by Sangyong Jeon, Peter Arnold (?), and Marco van Leeuwen.]

These two formalisms valid in the multiple soft scattering limit differ in essential aspects: AMY is based on a rigorous field theoretic formulation and a specific perturbative picture of the quark-gluon plasma, but does not account for vacuum radiation and its interference with the medium induced radiation; BDMPS-Z does account for vacuum-medium radiation interference, but is based on a representation of the medium as a collection of static scattering centers. Among the salient discussion points are:

- AMY does not contain interference between vacuum and medium induced radiation;
- AMY implements exact energy and momentum conservation, both in the elementary process and in the radiative cascade;
- AMY treats the medium dynamically, not as collection of static scattering centers;
- Langevin dynamics is not a good approximation for collisional energy loss;
- AMY and BDMPS both assume collinearity of the radiation.

### D. WHDG/ASW-OE and BDMPS-Z

[Coordinated by Marta Verweij and Marco van Leeuwen.]

The multiple soft scattering approximation is compared with the opacity expansion formalism. For this work the following energy loss models are used:

*Note: It would be good if we can agree on a useful naming convention for all these energy loss models.*

- **Salgado-Wiedemann multiple soft scattering** (BDMPS-Z/ASW-MS) as reported in reference [? ].
- **Salgado-Wiedemann Opacity Expansion** (ASW-OE): The single hard scattering approximation as described in [? ]. It consists of an incoherent superposition of a few single hard scatterings. Originally with a fixed value for  $L/\lambda$ . For this work  $L/\lambda$  is calculated from the temperature  $T$  in the medium.
- **Wicks-Horowitz-Djordjevic-Gyulassy Opacity Expansion** (WHDG rad)[? ]: this model is based on the GLV opacity expansion [? ] and calculates the radiated gluon energy starting from an analytical expression for the single gluon emission spectrum to all orders of opacity. For the single gluon spectrum there is a smoothly cut-off given by the parton energy. Using the average number of emitted gluons the  $P(\Delta E)$  is calculated for a parton. The energy loss is calculated following the DGLV formulas for radiative energy loss as reported in appendix B of [? ] (WHDG).

*Note: Probably the following two sections (Relation between  $\hat{q}$ ,  $\mu$  and  $\lambda$  and Suppression factor in a brick) should be moved to earlier in the paper.*

#### 1. Relation between $\hat{q}$ , $\mu$ and $\lambda$

The transport coefficient  $\hat{q}$  is defined by [? ? ]

$$\hat{q} = \int_{q_{\perp} < q_{max}} d^2 q_{\perp} \frac{d\Gamma_{el}}{d^2 q_{\perp}} q_{\perp}^2, \quad (18)$$

in which  $\Gamma_{el}$  is rate for elastic collisions in the plasma,  $q_{\perp}$  is transverse momentum which the parton loses in such a collision and  $q_{max}$  is the ultraviolet cut-off. In the eikonal limit,  $q_{\perp} \gg T$ , the elastic cross section is

$$\frac{d\Gamma_{el}}{d^2q_{\perp}} = \frac{C_R}{(2\pi)^2} \frac{g^4 \mathcal{N}}{q_{\perp}^4}, \quad (19)$$

with  $\mathcal{N}$  the density of the plasma and  $C_R$  the Casimir factor. Combining equation 19 with equation 18 gives

$$\hat{q} = 4\pi\alpha_s^2 C_R \mathcal{N} \ln\left(\frac{q_{max}^2}{\mu^2}\right) = \frac{72 \cdot 1.202 \cdot \alpha_s^2}{\pi} T^3 \ln\left(\frac{q_{max}^2}{\mu^2}\right), \quad (20)$$

with  $\mu = \sqrt{4\pi\alpha_s}T$  the Debeye mass and  $q_{max}$  the upper limit of the integration. Equation 20 is used to calculate the transport coefficient in the multiple soft scattering approximation and serves as a direct input for the calculation of the parton energy loss. For the opacity expansion formalism  $\mu$  and  $\lambda$  are the input parameters and  $\hat{q}$  has to be expressed in them to make a direct comparison between the different formalisms. To calculate  $1/\lambda$  we take

$$\frac{1}{\lambda} = \int d^2q_{\perp} \frac{d\Gamma_{el}}{d^2q_{\perp}} = \frac{4\pi C_R \alpha_s^2 \mathcal{N}}{\mu^2} = \frac{72 \cdot 1.202 \cdot \alpha_s^2}{\pi \mu^2} T^3. \quad (21)$$

Combining equation 21 with equation 20 the following relation between  $\hat{q}$ ,  $\mu$  and  $\lambda$  arises

$$\hat{q} = \frac{\mu^2}{\lambda} \ln(q_{max}^2/\mu^2), \quad (22)$$

with  $q_{max} = \sqrt{ET}$ .

## 2. Suppression factor in a brick

The measured hadron spectra at RHIC follow a power law:  $\frac{dN}{dp_t} = \frac{1}{p_t^n}$ . If each hadron loses  $\epsilon$  energy the hadron spectrum will look as following:

$$\frac{dN}{dp_t} = \frac{1}{[(1-\epsilon)p_t]^n} \frac{dp_t'}{dp_t} = \frac{1}{(1-\epsilon)^{n-1} p_t^n}, \quad (23)$$

with  $p_t'$  the momentum of the hadron after radiating energy in the medium. Since a hadron does not lose a fixed amount of energy but there is a probability to lose a certain amount of energy, the nuclear modification factor  $R_{AA}$  can be approximated by the weighted average energy loss:

$$R_n = \int_0^1 d\epsilon (1-\epsilon)^{n-1} P(\epsilon), \quad (24)$$

in which  $\epsilon = \Delta E/E$ . Because for RHIC energies the hadron  $p_t$  spectrum is very similar to a power law spectrum with  $n = 6.5$  for  $p_t > 2$ . GeV/c [?]  $R_7$  will be used as an approximation for  $R_{AA}$ .

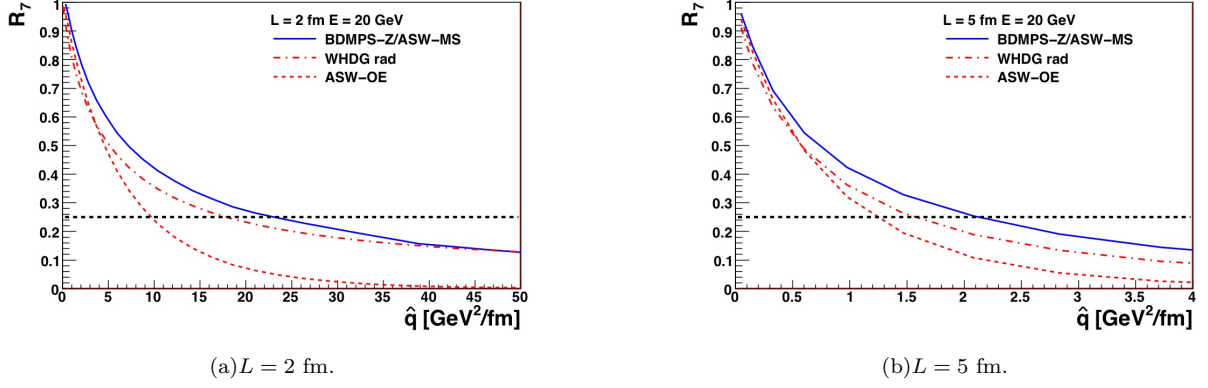


FIG. 11: Correlation between  $R_7$  and  $\hat{q}$  for a primary quark with  $E = 20$  GeV for different energy loss formalisms. The horizontal black dashed line indicates  $R_7 = 0.25$ .

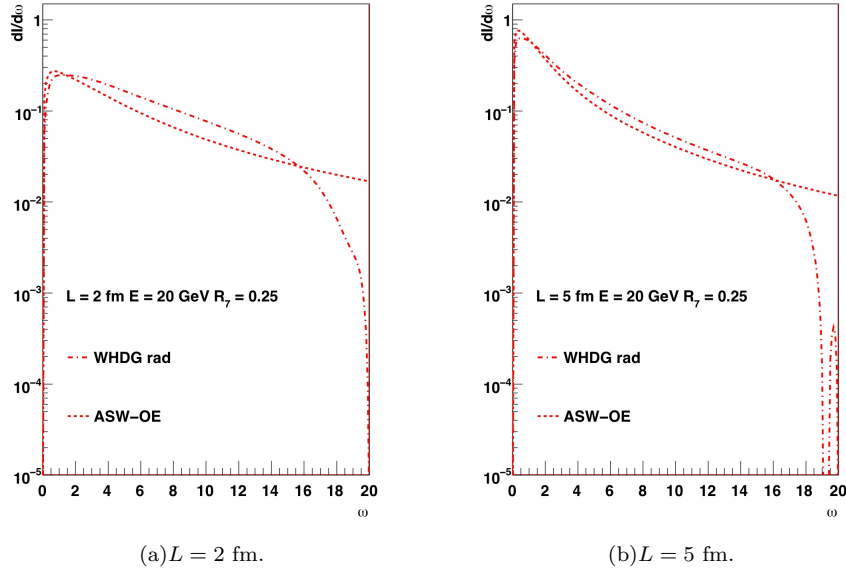


FIG. 12: The inclusive gluon spectrum for quarks with  $E = 20$  GeV. *Note: Spectra for BDMP5-Z/ASW have to be added. We will request ASW for data tables when we agree on the proposed definitions for  $\hat{q}$  and  $R_7$ .*

Figure 11 shows the correlation between  $R_7$  and  $\hat{q}$  for a quark with  $E = 20$  GeV for two different bricks of length  $L = 2$  fm and  $L = 5$  fm. The input parameters to calculate the energy loss in the different models depend on  $T$  and  $L$ . For the calculation of  $\hat{q}$  equations 20 and 22 are used with  $q_{max} = \sqrt{ET}$ . From this figure can be seen that both opacity expansion formalisms lose more energy at the same density compared to the multiple soft scattering approximation. For a brick of  $L = 2$  fm a  $R_7$  value of 0.25 is reached at  $\hat{q} = 17.9$  GeV<sup>2</sup>/fm for WHDG and at  $\hat{q} = 9.7$  GeV<sup>2</sup>/fm for ASW-OE while the the multiple soft scattering approximation needs  $\hat{q} = 23.1$  GeV<sup>2</sup>/fm to reach the same suppression. For a brick of  $L = 5$  fm  $\hat{q}$  has to be 1.58, 1.25 and 2.13 GeV<sup>2</sup>/fm for respectively WHDG, ASW-OE and BDMPS to have a suppression of  $R_7 = 0.25$ . In order to reach a similar suppression as measured at RHIC [? ? ?] with the multiple soft scattering approximation and the opacity expansion there is roughly a factor 2 difference in  $\hat{q}$ . The larger energy loss in the opacity expansion formalism is mainly caused by the smaller discrete weights of the energy loss probability distribution under the same medium conditions.

In figure 12 the inclusive gluon spectra for two bricks of  $L = 2$  and  $L = 5$  fm are shown. These spectra correspond to a suppression factor  $R_7 = 0.25$ . Therefor the medium density of each model has been taken differently, see figure 11. The single gluon spectrum WHDG does not have a tail because in the WHDG calculation the single gluon spectrum is modified by a factor which smoothly cuts off the spectrum at the energy of the incoming quark  $E = 20$  GeV.

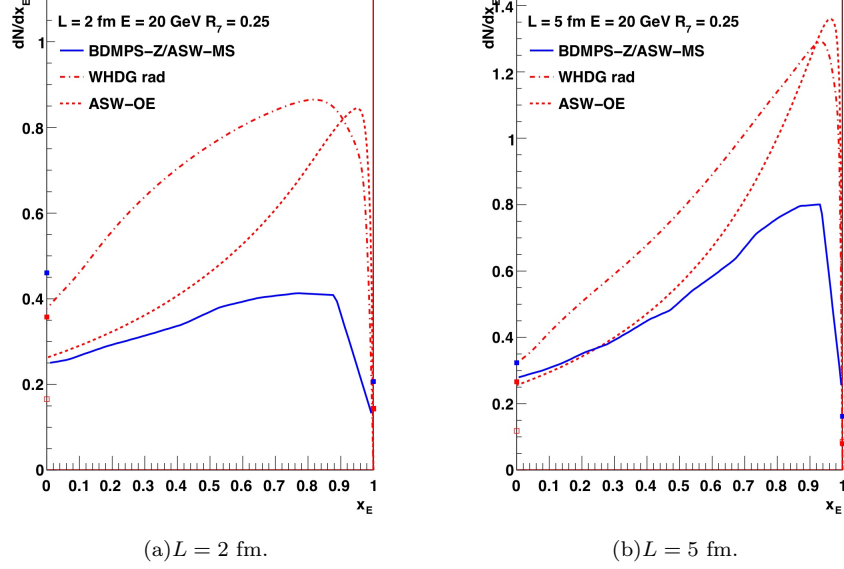


FIG. 13: The final quark energy spectrum as function of  $x_E = 1 - \epsilon$ . The squares at  $x_E = 0$  indicate the probability that a quark is absorbed and at  $x_E = 1$  the probability that a quark does not interact with the medium. Solid blue squares: BDMPS-Z/ASW-MS. Open red squares: WHDG. Solid red squares: ASW-OE.

Figure 13 shows the final quark energy spectrum as function of  $x_E = 1 - \epsilon$  for the two bricks of different lengths and  $R_7 = 0.25$ . In the same figure the probability that a parton is absorbed in the medium is indicated by the squares at  $x_E = 0$ . At  $x_E = 1$  the corresponding discrete weights for all three models are given. The discrete and the absorption rates of the multiple soft scattering approximation are larger than for the opacity expansions. It seems that the continuous part of the energy loss probability distribution is more relevant in the opacity expansion. The BDMPS model seems to behave more like a *black-white* scenario.

Figure 14 shows contours for different suppression factors  $R_7$  as function of the in-medium path length  $L$  and the transport coefficient  $\hat{q}$ . Since the typical size of a nucleus is  $L \sim 5$  fm, the relevant path lengths are  $L \lesssim 5$ . In this region a relatively small difference in  $L$  results in a very large difference in  $\hat{q}$  for a fixed value of  $R_7$ . A scaling in  $L$  is much more efficient than a scaling in medium density because the energy loss scales with  $\hat{q}L^2$ . To achieve a significant difference in the fraction of lost energy a large step in medium density is needed. The WHDG model requires larger combinations of  $\hat{q}$  and  $L$  than ASW-OE in order to achieve the same suppression factor. This is due to the smooth cut-off in the single gluon spectrum at the quark energy ( $E = 20$  GeV) in the WHDG model, cf. figure 11. For small  $\hat{q}$  and small  $L$  this is not a dominant effect because the tail of the single gluon energy distribution is shorter which makes the single gluon spectra of ASW-OE and WHDG and thus the energy loss probability distribution less different. This is also represented in the crossing points at small  $\hat{q}$  of the two opacity expansion curves in figure 11.

The multiple soft scattering approximation requires larger values for  $\hat{q}$  and  $L$  than both opacity expansion formalisms in order to achieve the same fraction of energy loss. The region in  $\hat{q}$  and  $L$  in which a parton survives is more limited for the opacity expansion than for the multiple soft scattering approximation. This is mainly due to the larger probability to lose no energy in the multiple soft approximation at the same medium density.

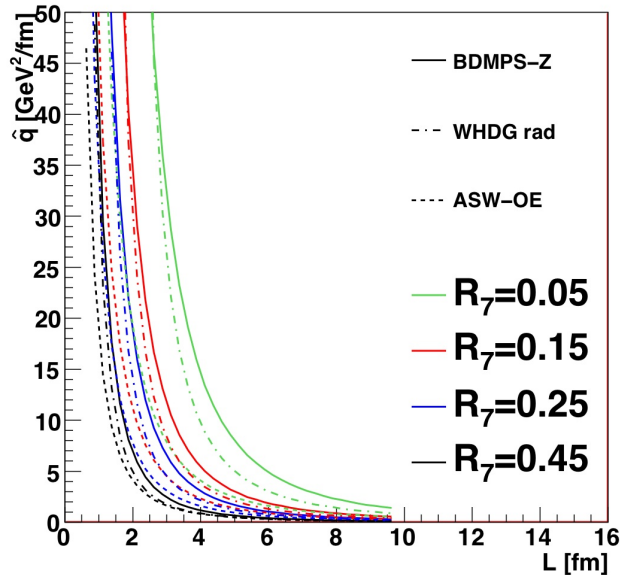


FIG. 14: In-medium path length versus transport coefficient for BDMPS (solid lines), WHDG (dashed dotted lines) and ASW-OE (dashed lines) energy loss models. The lines represent isolines from brick calculations for  $R_7 = 0.05$  (green), 0.15 (red), 0.25 (blue) and 0.45 (black). This is for quarks with  $E = 20$  GeV.

#### IV. BASELINE PLOTS

This section will present and discuss the plots generated by the different formalisms for various parameters of the QGP Brick challenge. For each model, we will show the following six plots:

1. The inclusive gluon spectrum  $dN_g/dx_E$  for the following parameters: primary parton = quark,  $L = 2$  fm,  $E = 20$  GeV,  $R_8 = 0.25$ ;
2. The inclusive gluon spectrum  $dN_g/dx_E$  for the following parameters: primary parton = quark,  $L = 5$  fm,  $E = 20$  GeV,  $R_8 = 0.25$ ;
3. The final spectrum  $dN_q/dx_E$  for the following parameters: primary parton = quark,  $L = 2$  fm,  $E = 20$  GeV,  $R_8 = 0.25$ ;
4. The final spectrum  $dN_q/dx_E$  for the following parameters: primary parton = quark,  $L = 5$  fm,  $E = 20$  GeV,  $R_8 = 0.25$ ;
5. For each of the models, the range of correlation between  $R_8$  and  $\hat{q}$  for a primary quark and  $L = 2$  fm,  $E = 20$  GeV;
6. For each of the models, the range of correlation between  $R_8$  and  $\hat{q}$  for a primary quark and  $L = 5$  fm,  $E = 20$  GeV.

For (1–4), the inclusive spectrum of gluons (quarks) at the end of the brick should be plotted. For gluons, this is the spectrum calculated from the “elementary” emission formula; for quarks, this requires the Poisson (or other) convolution with the probabilistic distribution of scatterers. [This interpretation needs to be confirmed.] For AMY, both  $dN_g/dx_E$  and  $dN_q/dx_E$  are obtained by solving the rate equations.

For (5) and (6), the whole range of correlation should be shown, when all other parameters of the jet quenching model are varied, keeping  $R_8$ ,  $L$ , and  $E$  fixed.

#### V. OUTLOOK

This section will summarize the limitations of the validity of the various first-generation formalisms and give estimates of the inherent uncertainties of their predictions that limit the current theory–data comparison. The

section will also describe the minimal requirements for all second-generation approaches, which hope to avoid the most serious of these limitations.

- 
- [1] Actually the ASW-SH implementation [?] is only in terms of the Poisson convoluted energy loss probability distribution, which we will discuss in detail further below. The comparison shown here actually comes from an independent numerical implementation of the massless ASW-SH formula by B. Cole that well reproduces the Poisson convolution results of [?].
- [2] In general one needs to consider the distribution in differences in distance between successive scattering centers. However at first order in opacity there is only one scattering center; as one may always set the initial value of  $z$  to 0,  $\rho(z)$  is the absolute distance to the first scattering center
- [3] In GLV and BDMPS (4) is used to neglect poles from propagators multiplied by  $\exp(-\mu\Delta z) \approx \exp(-\mu\lambda) \ll 1$ , where  $\Delta z$  is the distance between successive scattering centers; this approach is probably invalid for  $L \lesssim \lambda \sim 1$  fm. On the other hand AMY uses the central limit theorem in its Langevin approach and corrections are likely for  $L \lesssim 30\lambda \sim 30$  fm; this extra long path length is also required by the neglect of the interference between vacuum and in-medium induced radiation.